Original Research

Investigation of Acupoint Specificity by Multivariate Granger Causality Analysis From Functional MRI Data

Yuanyuan Feng, PhD,[1] Lijun Bai, PhD,[1] Wensheng Zhang, PhD,[1]* Ting Xue, PhD,[2] Yanshuang Ren, PhD,[3,4] Chongguang Zhong, PhD,[1] Hu Wang, PhD,[1] Youbo You, PhD,[1] Zhenyu Liu, PhD,[1] Jianping Dai, MD,[5] Yijun Liu, PhD,[6] and Jie Tian, PhD[1,2]

Purpose: To investigate the acupoint specificity by exploring the effective connectivity patterns of the poststimulus resting brain networks modulated by acupuncture at the PC6, with the same meridian acupoint PC7 and different meridian acupoint GB37.

Materials and Methods: The functional MRI (fMRI) study was performed in 36 healthy right-handed subjects receiving acupuncture at three acupoints, respectively. Due to the sustained effects of acupuncture, a novel experimental paradigm using the nonrepeated event-related (NRER) design was adopted. Psychophysical responses (deqi sensations) were also assessed. Finally, a newly multivariate Granger causality analysis (mGCA) was used to analyze effective connectivity patterns of the resting fMRI data taken following acupuncture at three acupoints.

Results: Following acupuncture at PC6, the red nucleus and substantia nigra emerged as central hubs, in comparison with the fusiform gyrus following acupuncture at GB37. Red nucleus was also a target following acupuncture at PC7, but with fewer inputs than those of PC6. In addition, the most important target following acupuncture at PC7 was located at the parahippocampus.

Conclusion: Our findings demonstrated that acupuncture at different acupoints may exert heterogeneous modulatory effects on the causal interactions of brain areas during the poststimulus resting state. These preliminary findings provided a clue to elucidate the relatively function-oriented specificity of acupuncture effects.

Key Words: acupuncture specificity; mGCA; fMRI; delayed effect

J. Magn. Reson. Imaging 2011; 34:31–42.

ORIGINATED IN ANCIENT China, acupuncture has currently been recognized in the Western medicine as an important complementary therapy (1). However, the mechanism underlying this traditional intervention has not been clear and needs further investigations. In the past decades, functional MRI (fMRI) has been used to study the anatomy and physiological function underlying the acupuncture.

Previous studies mainly focused on the neural activities involving the acute effects of acupuncture (2–4). Hui and colleagues reported that acupuncture can exert modulatory effects on the limbic system and subcortical gray structures in the human brain (3). The modulation of cerebellar activities underlying the acupuncture stimulation was further proved later (4). One recent report has provided additional evidence to support that acupuncture can modulate the limbic-paralimbic-neocortical network (2). Overall, these studies generally adopted the block-designed fMRI paradigm, and therefore the temporal changes in the blood oxygen level-dependent (BOLD) signal as predicted by the generalized linear model (GLM) conform to the "on-off" specifications. According to the theory of the traditional Chinese medicine (TCM), acupuncture can induce long-lasting effects even after the needling

[1]Key Laboratory of Complex Systems and Intelligence Science, Institute of Automation, Chinese Academy of Sciences, Beijing, China.

[2]Life Science Research Center, School of Life Sciences and Technology, Xidian University, Xi'an, Shaanxi, China.

[3]Department of Radiology, Xuanwu Hospital, Capital Medical University, Beijing, China.

[4]Department of Radiology, Guang'anmen Hospital, Chinese Academy of Traditional medicine, Beijing, China.

[5]Department of Radiology, Beijing Tiantan Hospital, Capital University of Medical Sciences, Beijing, China.

[6]Departments of Psychiatry and Neuroscience, McKnight Brain Institute, University of Florida, Gainesville, Florida, USA.

Contract grant sponsor: the Project for the National Key Basic Research and Development Program (973) under Grant No. 2011CB707700, the Chinese Academy of Sciences; Contract grant number: KGCX2-YW-129; Contract grant sponsor: the National High Technology Research and Development Program of China (863 Program); Contract grant number: 2008AA01Z121; Contract grant number: 2007AA01Z338; Contract grant sponsor: the National Natural Science Foundation of China; Contract grant number: 30873462; Contract grant number: 30970774; Contract grant number: 60901064; Contract grant number: 90924026; Contract grant number: 81071137; Contract grant number: 81071217.

Drs. Feng and Bai contributed equally to this work.

*Address reprint requests to: W.Z., Institute of Automation, Chinese Academy of Science, P.O. Box 2728, Beijing, 100190, China. E-mail: wensheng.zhang@ia.ac.cn

Received May 20, 2010; Accepted March 3, 2011.

DOI 10.1002/jmri.22585
View this article online at wileyonlinelibrary.com.

manipulation being terminated (5). Considering such delayed effect, the "off-state" in the block design may remain some effects of acupuncture, and cannot ideally return to the baseline level (6). In addition, one recent study has already pointed that neural responses induced by acupuncture have the saliently time-varying characteristics (6–9). This temporal aspect of the BOLD response to acupuncture may violate the assumptions of the block-designed GLM estimates, which may be susceptible to errors of statistical significance (6). Therefore, a newly experimental paradigm namely the NRER design was adopted to explore the neural responses induced by acupuncture. This design incorporates the sustained phase which focuses on the dynamic of acupuncture-related brain activities. Considering the sustained effects of acupuncture, the NRER design may be more suitable to elucidate its specific mechanism underlying acupuncture.

Several studies have paid attention to the sustained effect of the acupuncture and its influence on the poststimulus resting state networks (8–12). Dhond et al revealed that acupuncture can influence intrinsic connectivity in the resting brain networks, i.e., default mode network (11). Our group has investigated the functional connectivity of brain networks involved in acupuncture and demonstrated that acupuncture can exert modulatory effect on the insula-anchored brain network during the poststimulus resting period (8). One recent study further proved the existence of a large anti-correlated functional connectivity networks of resting brain modulated by acupuncture (12). These studies demonstrated the existence of function-guided brain networks underlying the specific effect of acupuncture. Most of them adopted the standard functional connectivity analysis, which was a kind of undirected graph analysis of temporal correlations between time series in different brain regions. However, little was known about the direction and strength of the information flow between these brain regions modulated by acupuncture. Further investigation of the interregional causal interactions may be helpful to explain the neurophysiological action underlying acupuncture. Recently, a newly multivariate Granger causality analysis (mGCA) has been introduced as an effective connectivity method to analyze causal relations among multiple brain areas from fMRI data (13–15). By exploring this approach to analyze the causal influences of the activated regions modulated by acupuncture, we can account for the acupuncture modulatory effects on multiple relevant regions simultaneously. Unraveling the organization of the large-scale cortical networks following acupuncture would pave the way to better understand the neurophysiological function underlying acupuncture.

In the present study, we combined mGCA (14) with the NRER design to evaluate the effective connectivity patterns among multiple brain regions during the poststimulus resting state following acupuncture at the PC6, with the same meridian acupoint PC7 and different meridian acupoint GB37. We examined the directionality and strength of causal influence between multiple brain regions following acupuncture at three acupoints to find whether there was the relatively specific modulatory effect underlying acupuncture at different acupoints. By detecting the specificity of brain effective connectivity underlying the same meridian and different meridian acupoints, we can provide further evidence to explore the functional specificity of acupuncture.

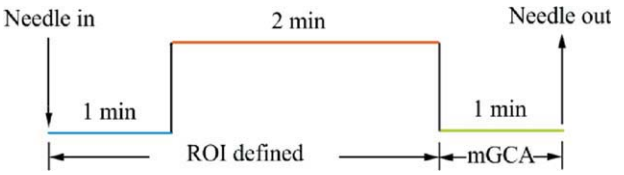

Figure 1. Experimental paradigm. The entire run for each acupoint lasted for 4 min. For statistical analyses, the signal intensity during the 1 min rest phase served as a control baseline for detecting the changes in signal intensity during acupuncture stimulation, thereby functionally defining the regions of interest. In addition, the data from the 1 min rest phase were used for mGCA. [Color figure can be viewed in the online issue, which is available at wileyonlinelibrary.com.]

MATERIALS AND METHODS

Subjects

Thirty-six healthy right-handed college students (18 males, aged 21.4 ± 1.3) were recruited from a homogeneous group to reduce intersubject variabilities. All subjects were acupuncture naïve according to the Edinburgh Handedness Inventory (16). After given a complete description of the study, each of the subjects signed the informed consent form. All subjects were free of any major medical illnesses, any head trauma, any neuropsychiatric disorders, any intake of prescription medications within the last month, as well as any contraindications for exposure to a high magnetic field. Subjects were allocated to receive once acupuncture at one of the three acupoints in a random sequence by using an envelope method, with the gender ratio balanced (analysis of variance, $P > 0.6$) among different groups. All protocols were approved by a local subcommittee on Human Studies.

Experimental Paradigm

All subjects underwent a resting state scan. The NRER scanning for every acupoint incorporated 2-min needling manipulations, preceded by a 1-min rest, and followed by another 1-min rest scanning (shown in Fig. 1). During the experiment, the subjects were instructed to keep their eyes closed and remain relaxed without engaging in any mental tasks. Each subject only received once acupuncture at one of the three acupoints in a random order: PC6 (Neiguan), located between the tendon of palmaris longus and flexor carpi radialis at a depth approximately 3 cm above the midpoint of the transverse crease of the wrist (17); PC7 (Daling), located between the tendons of the long palmar muscle and radial flexor muscle at the midpoint of the crease of the wrist (18); GB37 (Guangming), located in the lateral aspect of the lower leg with needle being inserted on the anterior border of the fibula (19). A sterile disposable 38 gauge

stainless steel acupuncture needle (0.2 mm in diameter and 40 mm in length) was used to deliver acupuncture stimulation. During acupuncture, the needle was rotated manually clockwise and counterclockwise for 1 min at a rate of 60 times per min by a balanced "tonifying and reducing" technique (3). The precise locations of needling, the presumed acupuncture effects, and the stimulation paradigm were not divulged. The procedure was performed by the same experienced and licensed acupuncturist on all subjects.

The subjects were questioned about aching, pressure, soreness, heaviness, fullness, warmth, coolness, numbness, tingling, dull or sharp pain and any other sensations they felt during the scan after each fMRI scanning (20,21). The questionnaire used a 10-point visual analogue scale (VAS), which was scaled at 0 = no sensation, 1–3 = mild, 4–6 = moderate, 7–8 = strong, 9 = severe and 10 = unbearable sensation. The subjects were excluded from further analysis if they experienced sharp pain (greater than the mean by more than 2 standard deviations) (20). None experienced the sharp pain among the 36 participants.

Data Acquisition and Analysis

MRI data were acquired using a 3.0 Tesla (T) Signa (GE) MR scanner. Head movements were prevented by a custom-built head holder. The images were parallel to the anterior commissure–posterior commissure line and covered the whole brain. Thirty-two axial slices were obtained using a T2*-weighted single-shot, gradient-recalled echo planar imaging (EPI) sequence (field of view [FOV] = 240 mm × 240 mm, matrix = 64 × 64, thickness = 5 mm, repetition time [TR] = 2000 ms, echo time [TE]= 30 ms, flip angle = 90°). After the functional run, high-resolution structural information on each subject was also acquired using three-dimensional (3D) MRI sequences with a voxel size of 1 mm^3 for anatomical localization (TR = 2.7 s, TE = 3.39 ms, matrix = 256 × 256, FOV = 256 mm × 256 mm, flip angle = 7°, slice thickness = 1 mm).

After that, all images were preprocessed using statistical parametric mapping (SPM5, http://www.fil.ion.ucl.ac.uk/spm/). First, the image data underwent slice-timing correction and realignment for head motions using least-squares minimization. None of the subjects had head movements exceeding 1 mm on any axis and head rotation greater than one degree. Thus all subjects (n = 36) were left. A mean image created from the realigned volumes was coregistered with the subject's individual structural T1-weighted volume image. Then, the standard MNI template provided by SPM5 was used in spatial normalization with resampling at 2 mm × 2 mm × 2 mm (22). In the end, the functional images were spatially smoothed with a 3D Gaussian kernel (FWHM = 6 mm).

Definition of Regions of Interest

Taking into account the sustained effects of acupuncture, the mean signal intensity of the resting period preceded by the active stimulation was taken as the baseline. For each subject, the difference in the BOLD response between stimulus and baseline conditions was estimated at every voxel across the whole brain volume by using the general linear model (GLM) in SPM5. The obtained t-maps at individual levels were then entered into the "random effect" group analysis framework by the one-sample t-test (d.f. = 11) summary statistic ($P < 0.001$, uncorrected). The statistical maps indicated the brain activation in response to acute effects of acupuncture stimuli, thereby functionally defining the regions of interest (ROIs). Each peak voxel with its nearest 10 neighbors was defined as a group ROI.

Considering the anatomical variance across subjects, subject-specific peak voxels and subject-specific ROIs were defined on individual t-maps as follows. The given group ROI was used as a mask and then, based on individual t-maps, the voxel with the largest t-value within this mask served as the subject-specific peak voxel. ROIs were selected based on the acupuncture-stimulation results. First, the time series corresponding to the poststimulus period of BOLD signal intensities from these selected ROIs were selected. Then, the time series were averaged across voxels within each ROI and normalized across subjects separately for each group to form a single vector per ROI. In this manner, we obtained a total of 25 ROI time series related to acupuncture stimulation for each acupoint for further analysis.

mGCA

In this study, we used mGCA to describe the effective connectivity in the postacupuncture resting brain (14). This approach detected causal interactions between brain regions by computing directed transfer function (DTF) from a multivariate autoregressive model of the time-course of selected ROIs. Based on the principle of Granger causality, the DTF was rendered in a multivariate formulation (23). Therefore the DTF can effectively model the inherently multivariate nature of neuronal networks. Preprocessed dataset were implemented using this method. The algorithm was coded in MATLAB7 (The MathWorks Inc.) and details were as follows.

First, we need to construct the multivariate autoregressive (MVAR) model of the times series. Let $X(t) = [x_1(t), x_2(t),\ldots, x_M(t)]$ be a matrix representing data from M ROIs, in which $x_i(t)$ is the time series corresponding to ith ROI. The MVAR model of order p is given by the following:

$$X(t) = \sum_{x-1}^{p} A(n)X(t-n) + E(t) \qquad [1]$$

Traditionally, the model order was determined using the Akaike information criterion (24). Here, a model order of one was chosen (14). $A(n)$ is the matrix of prediction coefficients composed of elements $a_{ij}(n)$. $E(t)$ is the vector corresponding to the residual errors. Then applying the Fourier transform to Eq. [1] is given as follows:

$$X(f) = A^{-1}(f)E(f) = H(f)E(f) \qquad [2]$$

Where

$$a_{ij}(f) = \delta_{ij} - \sum_{n=1}^{p} a_{ij}(n)e^{-i2\pi fn} \text{ and } H(f) = A^{-1}(f) \quad [3]$$

Here, δ_{ij} is the Dirac-delta function, which is 1 when i = j and 0 otherwise. Also, i = 1. . .M, j = 1. . .M. H(*f*) is the frequency domain transfer matrix and $h_{ij}(f)$ represents its ith row and jth column element. $h_{ij}(f)$ is defined as the nonnormalized DTF (25) corresponding to the influence of ROI j onto ROI i. The direct DTF (dDTF) was obtained by multiplying $h_{ij}(f)$ with the partial coherence between ROIs i and j (25). This operation ensures that direct connections are emphasized and mediated influences are de-emphasized. To calculate the partial coherence, the cross-spectra were computed as follows:

$$S(f) = H(f)VH^{*}(f) \quad [4]$$

Here, V is the variance of the matrix E(*f*), and the asterisk denoted transposition and complex conjugation. Then we obtained the partial coherence between ROIs i and j:

$$\upsilon_{ij}(f) = \frac{M_{ij}^{2}(f)}{M_{ii}(f)M_{ij}(f)} \quad [5]$$

where $M_{ij}(f)$ is the minor obtained by removing the ith row and jth column from the matrix S (26). The partial coherence lies in the range of (0, 1). Here, a value of 0 indicates no direct association between the ROIs with the influence of all other ROIs removed. While if the value is 1 indicates there exists complete direct association. Finally the dDTF is defined as the sum of all frequency components of the product of the non-normalized DTF and partial coherence as given in the equation below:

$$dDTF_{ij} = \sum_{f} h_{ij}(f)\upsilon_{ij}(f) \quad [6]$$

In the end, we obtained the value of dDTF, which only reflects the magnitude of causal influence between the ROIs.

The statistical significance of the path weights was ascertained using surrogate data (25,27). Surrogate data were generated by randomizing the phase of the original time series spectrum while retaining its magnitude. A null distribution was obtained by generating 2500 sets of surrogate data and calculating the dDTF (for every connection) from these 2500 datasets. The dDTF value obtained from the original time series was verified using with the null distribution for a one-tailed test with the significant a *P*-value of 0.05. The effective connectivity network of the 25 ROIs was constructed by visualizing the significant dDTF ($P < 0.05$) obtained after running the statistical significant test. Additionally, we adopted In-Out degree to compare the effective connectivity network for three acupoints (28). The In-Out degree of a node is defined as the difference between its In-degree (the number of causal in-flows) and Out-degree (the number of causal out-flows). In-Out degree can identify hub regions that have important causal effects on network dynamics (28).

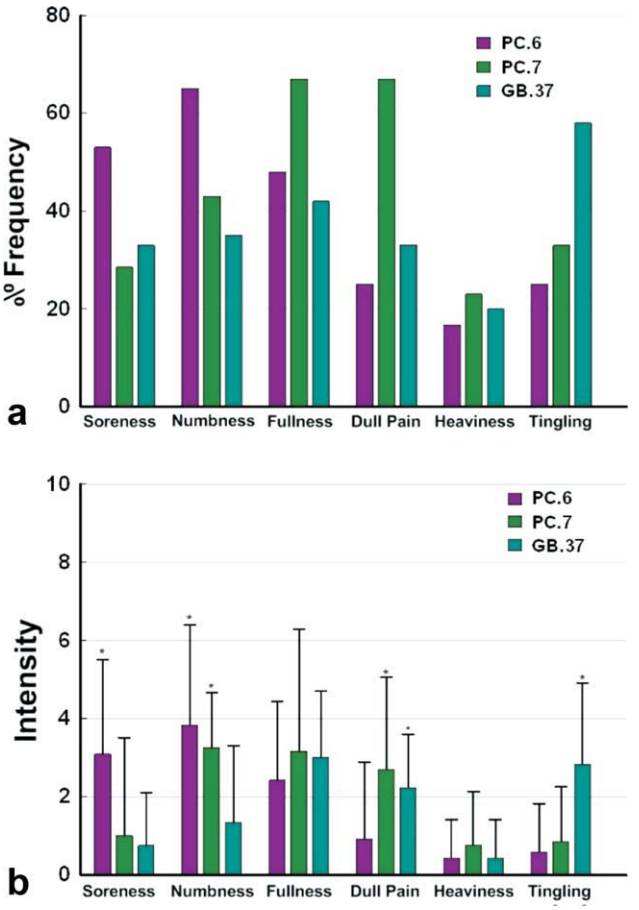

Figure 2. Averaged psychophysical response (N = 36). **A**: The percentage of subjects who reported having experienced the given sensation (at least one subject experienced the seven sensations listed). **B**: The intensity of reported sensations measured by an average score (with standard error bars) on a scale from 0 denoting no sensation to 10 denoting an unbearable sensation. *Denoting significant differences under Fisher's exact test ($P < 0.005$). [Color figure can be viewed in the online issue, which is available at wileyonlinelibrary.com.]

RESULTS

Psychophysical Results

In this study, the prevalence of deqi sensation was expressed as the percentage of individuals in the group that reported the given sensations (Fig. 2A). No difference was found in regard to the prevalence of the listed sensations elicited by acupuncture stimulation ($P > 0.05$) when grouped across all acupoints. However, there were some differences with respect to the type of sensations. In the case of PC6, soreness was 53%, seemed more frequent than the case of PC7 and GB37 which were 28% and 33%. Numbness was in the same case with soreness (65% versus 43% and 35%). Following acupuncture at PC7, fullness was 67%, occurred more commonly than PC6 and GB37 which were 48% and 42%. Compared with PC6 and GB37, dull pain was also in the same case with

Table 1
Coordinates and t Score of the Peak Voxel Within-Group ROIs Following Acupuncture at PC6, PC7 and GB37 ($P < 0.001$, Uncorrected)

	PC6						PC7						GB37					
		Talairach			t	V		Talairach			t	V		Talairach			t	V
Regions	Hem	x	y	z	value	voxels	Hem	x	y	z	value	voxels	Hem	x	y	z	Value	Voxels
FGM	R	8	-61	-19	-3.76	21	R	6	-56	-22	-2.73	3	R	6	-48	-19	3.38	8
Culmen	R	12	-53	-12	-4.82	413	R	10	-34	-15	-5.20	443	L	-44	-44	-20	4.49	143
Uvula	R	32	-77	-26	4.03	57	L	-6	-71	-27	-3.58	23	R	32	-77	-26	4.03	57
Nodule	R	10	-63	-24	-2.99	22	R	2	-56	-27	-4.02	82	R	2	-56	-27	-4.02	12
AMY	R	22	-4	-12	-4.28	87	L	-18	-8	-11	5.49	51	L	-18	-8	-11	5.49	51
PH	L	-26	-53	-6	-2.82	4	L	-12	-37	-2	-4.88	86	L	-22	-33	-2	6.39	33
HIPP	L	-28	-41	4	-2.84	1	L	-28	-35	-3	-2.74	2	L	-28	-14	-11	3.22	15
Insula	R	40	-6	2	-6.68	146	R	42	-38	18	-3.38	34	R	32	-27	11	3.77	20
RN	R	8	-22	-4	-2.95	4	R	4	-22	-4	-4.96	31	L	-6	-22	-4	3.33	3
SN	R	12	-22	-7	-3.21	6	R	8	-12	-8	-3.37	14	R	16	-20	-4	5.00	25
PTM	R	28	-16	-6	-3.59	19	L	-24	-11	13	-2.74	1	L	-24	-11	13	6.31	249
VPLN	L	-18	-17	3	-4.31	45	L	-22	-21	8	-2.86	4	L	-18	-19	1	5.08	39
VPMN	L	-16	-23	5	5.37	13	L	-16	-21	8	-2.85	3	L	-16	-23	5	5.37	13
CD	R	22	-34	16	-5.25	17	R	24	-36	13	-3.15	13	L	-32	-33	2	3.38	5
HYPO	L	-8	-6	-3	-2.84	3	L	-8	-6	-3	-2.84	3	L	-8	-6	-3	-2.84	3
Cuneus	L	-24	-55	-7	-3.43	19	R	16	-88	36	-4.75	40	L	-16	-97	9	3.83	30
FG	L	-36	-47	-14	-3.77	55	R	-42	-87	-26	-5.37	41	L	-44	-40	-18	5.61	59
MOG	L	-18	-87	17	3.77	16	L	38	-17	6	-3.28	8	L	-18	-87	17	3.77	16
SII	R	65	-20	36	-4.54	144	R	67	-19	18	-3.33	5	R	51	-15	54	5.04	53
SMA	R	61	-17	41	-5.30	20	R	20	-25	53	-3.85	3	L	-51	-4	35	7.91	36
DLPFC	R	57	18	3	-2.68	2	R	57	18	3	-2.68	2	R	59	22	19	4.73	67
IPL	L	-40	-29	38	-3.42	25	R	65	-42	22	-3.74	14	R	32	-50	54	4.18	5
ACC	L	-20	-16	38	-3.00	3	R	4	11	22	-3.05	4	R	4	11	22	-3.05	4
PCC	L	-46	-42	-15	-2.81	5	R	6	-28	25	-2.95	4	L	-6	-34	22	8.05	17
MTG	L	-65	-29	-4	-4.95	23	L	-65	-29	-4	-4.95	23	R	40	-55	25	5.54	116

Hem = hemisphere; FGM = fastigium; AMY = amygdala; PH = parahippocampal gyrus; HIPP = hippocampus; RN = red nucleus; SN = substania nigra; PTM = putamen; VPLN = ventral posterior lateral nucleus; VPMN = ventral posterior medial nucleus; CD = caudate; HYPO = hypothalamus; FG = fusiform gyrus; MOG = middle occipital gyrus; SII = secondary somatosensory cortex; SMA = supplementary motor area; DLPFC = dorsolateral prefrontal cortex; IPL = inferior parietal lobule; ACC = anterior cingulate cortex; PCC = posterior cingulate cortex; MTG = middle temporal gyrus.

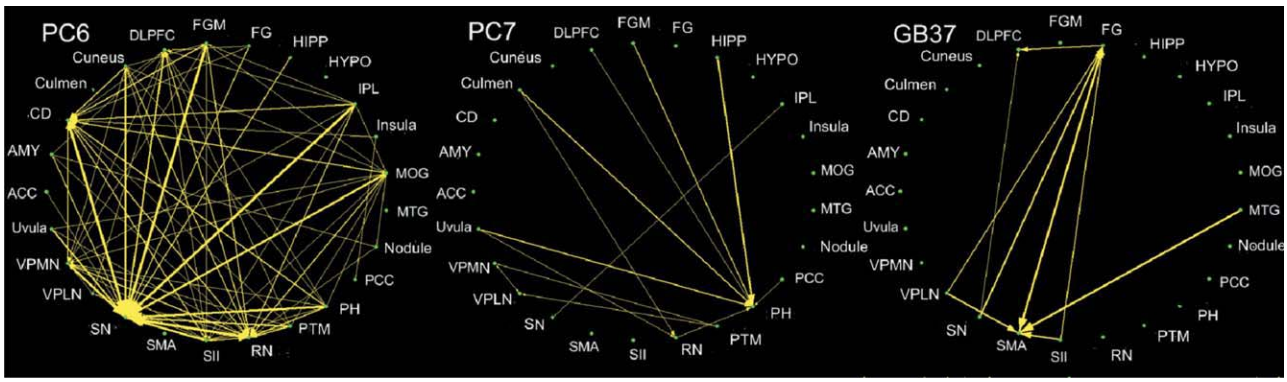

Figure 3. Multivariate Granger causality relationships with significant connections ($P < 0.05$) following acupuncture at PC6, PC7, and GB37. Relative strength of path weights (in arbitrary units) was indicated by the width of the arrows. Abbreviations: Hem, hemisphere; ACC, anterior cingulate cortex; AMY, amygdala; CD, caudate; DLPFC, dorsolateral prefrontal cortex; FGM, fastigium; FG, fusiform gyrus; HIPP, hippocampus; HYPO, hypothalamus; IPL, inferior parietal lobule; MOG, middle occipital gyrus; MTG, middle temporal gyrus; PCC, posterior cingulate cortex; PH, parahippocampal gyrus; PTM, putamen; RN, red nucleus; SII, secondary somatosensory cortex; SMA, supplementary motor area; SN, substania nigra; VPLN, ventral posterior lateral nucleus; VPMN, ventral posterior medial nucleus. [Color figure can be viewed in the online issue, which is available at wileyonlinelibrary.com.]

fullness (67% versus 25% and 33%) following acupuncture at PC7. In contrast, tingling was saliently more frequent for GB37 than PC6 and PC7 (58% versus 25% and 33%). The average stimulus intensities (mean ± SE) were approximately similar during acupuncture on PC6 (1.85 ± 1.80), PC7 (1.93 ± 2.03) and GB37 (1.83 ± 1.79) (Fig. 2B). However, soreness was more intense for PC6 than PC7 and GB37 ($P < 0.005$) while dull pain was stronger for PC7 and GB37 compared with PC6 ($P < 0.005$). In addition, numbness was more intense for PC6 and PC7 than GB37 ($P < 0.005$) while tingling exhibited more intense for GB37 compared with PC6 and PC7 ($P < 0.005$).

mGCA Result of Resting Brain Networks Modulated by Acupuncture at Three Acupoints

For bilaterally activated regions, we only selected the hemisphere anatomical area with a more significant t value as the representative ROI (shown in Table 1). The mGCA was performed on the averaged time series of voxels within each ROI, separately for each acupoint during the poststimulus phase. Effective connectivity graphs were constructed using the thickness of connecting lines and arrows to indicate the strength and direction of the causal influences (indicated in Fig. 3). Only links that showed significant effective connectivity were presented in the network ($P < 0.05$). Graphs were visualized using Pajek software (www.vlado.fmf.uni-lj.si/pub/networks/pajek). The In-Out degrees of three effective connectivity networks were sorted in a descending order as shown in Figure 4. Only the brain regions with a nonzero value of In-Out degree were listed.

Following acupuncture at PC6, the mGCA result showed that the substantia nigra and red nucleus emerged as central hubs. The substantia nigra received causal inflows from almost all other nodes in the brain network, including the amygdala, caudate, fastigium, hippocampus, parahippocampal gyrus (PH), red nucleus, secondary somatosensory cortex (SII) and uvula. In addition, the red nucleus received causal inflows from more than half regions in the brain network, primarily from the caudate, fastigium, substantia nigra, and SII. Of interest, we found that the red nucleus and substantia nigra were not only central hubs but also have significant causal influence with each other. The path weights of mGCA result for PC6 were tabulated in Table 2 with significant connections shown in red color.

The brain regions with extensive causal interactions following acupuncture at PC6 were mainly located at the limbic/paralimbic-cerebellum and subcortical areas as mentioned above. Of interest, several of these brain regions (the fastigium, hippocampus, PH and uvula) also have remarkably causal interactions following acupuncture at PC7. Furthermore, the red nucleus received two significant causal inflows from the culmen and uvula. In addition, the PH was a significant target, receiving causal inflows from the hippocampus, uvula, culmen and fastigium. In contrast, the brain regions with extensive causal interactions following acupuncture at GB37 were primarily located at the vision-related cortex (the fusiform gyrus), with limited extent of the limbic system. The fusiform gyrus received causal inflows primarily from the SII, thalamus (ventral posterior lateral nucleus [VPLN], ventral posterior medial nucleus [VPMN]). Moreover, we identified that several brain areas (the insula and nodule) only have causal interactions following acupuncture at PC6 compared with PC7 and GB37. The path weights of mGCA result for PC7 and GB37 were, respectively, tabulated in Tables 3 and 4 with significant connections shown in red color.

DISCUSSION

In this study, a newly mGCA combined with a novel NRER design were used to investigate the specific effective connectivity during the poststimulus resting period following acupuncture at PC6, PC7, and GB37. Our results demonstrated that acupuncture at

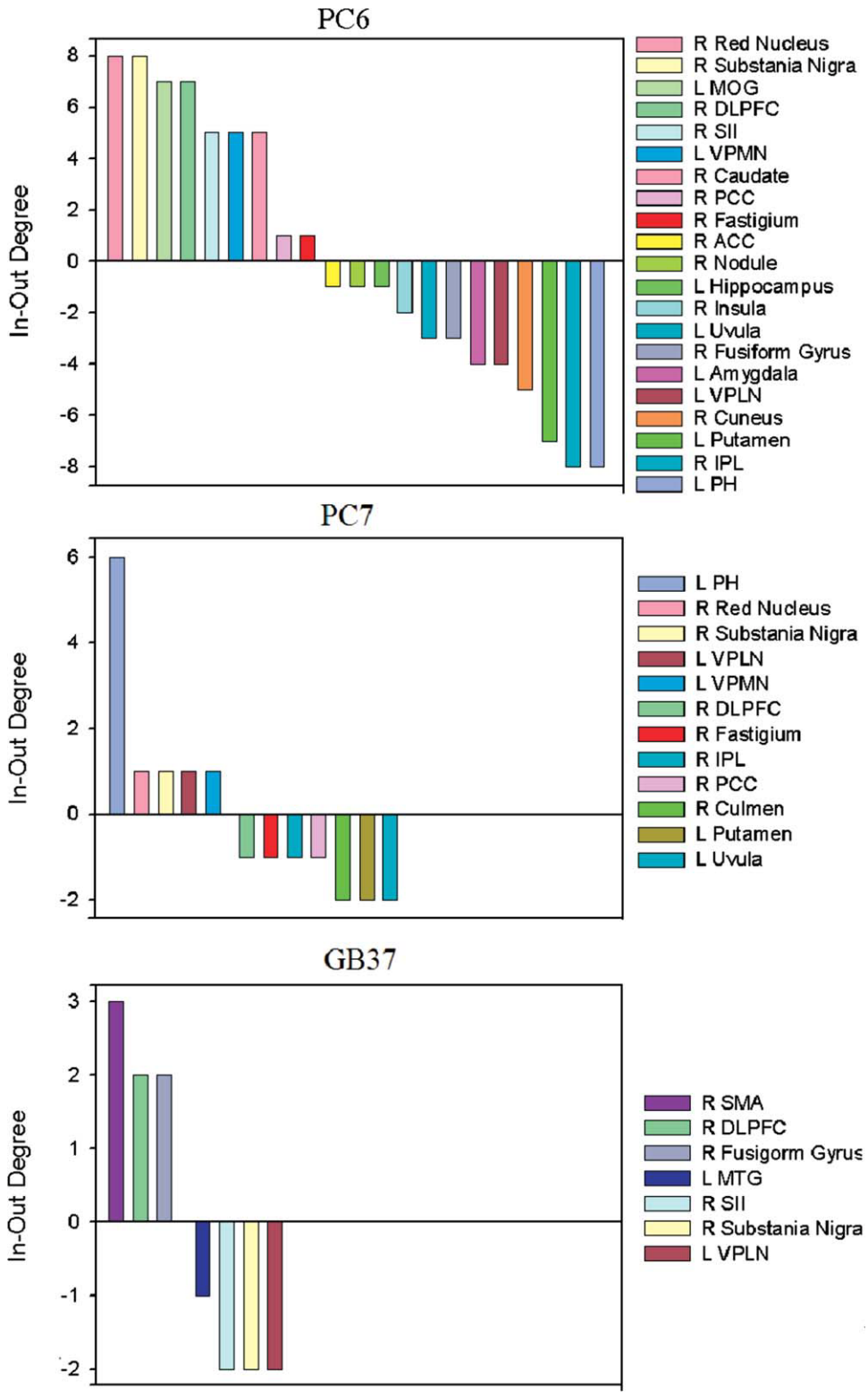

Figure 4. Ranking of the In-Out degrees of the effective connectivity network following acupuncture at each acupoint in a descending order. The In-Out degree of a node is defined as the difference between its In-degree (the number of causal in-flows) and Out-degree (the number of causal out-flows). Only the brain regions with a nonzero value of In-Out degree are listed here. Abbreviations: L, left hemisphere; R, right hemisphere; MOG, middle occipital gyrus; DLPFC, dorsolateral prefrontal cortex; SII, secondary somatosensory cortex; VPMN, ventral posterior medial nucleus; PCC, posterior cingulate cortex; ACC, anterior cingulate cortex; VPLN, ventral posterior lateral nucleus; IPL, inferior parietal lobule; PH, parahippocampal gyrus; SMA, supplementary motor area; MTG, middle temporal gyrus.

different acupoints may exert heterogeneous modulatory effects on the causal interactions of brain areas during the poststimulus resting state. As a peripheral input to transducing signals into the brain, acupuncture may induce the reorganization of the effective connectivity across different neural subsystems. These different effective connectivity patterns may be related to the special effects of acupuncture in clinical settings. Our findings may be helpful to understand the basic neurophysiological mechanisms underlying the functional specificity of acupuncture.

Several studies have begun to gaze on the modulatory effect of acupuncture on the resting brain networks, primarily using the functional connectivity analysis (8–12). Popular functional connectivity analysis primarily focused on the correlation patterns

Table 2
Path Weights (Arbitrary Units) From Multivariate Granger Causality Analyses of PC6

	ACC	AMY	CD	Culmen	Cuneus	DLPFC	FGM	FG	HIPP	HYPO	IPL	Insula	MOG	MTG	Nodule	PCC	PH	PTM	RN	SII	SMA	SN	VPLN	VPMN	Uvula
ACC	0.30	0.03	0.37	0.06	0.04	0.50	0.19	0.21	0.03	0.00	0.01	0.00	0.00	0.02	0.02	0.00	0.06	0.01	0.50	0.08	0.07	**1.34**	0.01	0.19	0.04
AMY	0.04	0.24	0.59	0.07	0.05	**0.80**	0.24	0.32	0.13	0.00	0.03	0.00	0.21	0.03	**0.27**	0.00	0.15	0.04	**0.90**	0.28	0.01	**1.92**	0.02	0.14	0.16
CD	0.04	0.05	2.79	0.07	0.23	**0.67**	**0.89**	0.27	0.12	0.00	0.03	0.04	**0.56**	0.00	0.07	0.24	0.19	0.09	**2.00**	**0.87**	0.03	**4.61**	0.15	**1.19**	0.28
Culmen	0.02	0.02	0.26	0.78	0.01	0.09	0.12	0.10	0.09	0.00	0.00	0.01	0.07	0.01	0.00	0.01	0.01	0.01	0.33	0.24	0.05	0.19	0.18	0.38	0.00
Cuneus	0.04	0.04	**2.06**	0.02	0.33	0.63	**0.64**	0.31	0.24	0.01	0.03	0.02	**0.41**	0.00	0.03	0.16	0.26	0.03	**1.66**	**0.61**	0.02	**4.07**	0.12	**0.99**	0.24
DLPFC	0.06	0.08	0.80	0.03	0.08	2.37	0.34	0.16	0.03	0.01	0.02	0.00	0.20	0.03	0.06	0.06	0.13	0.06	**1.56**	**0.56**	0.02	**2.72**	0.31	**0.89**	0.09
FGM	0.05	0.05	**2.40**	0.09	0.19	0.78	1.03	0.23	0.08	0.00	0.03	0.04	0.43	0.00	0.11	0.17	0.15	0.10	**2.20**	**0.90**	0.02	**4.75**	0.21	**1.21**	0.27
FG	0.10	0.12	**1.20**	0.12	0.16	**0.59**	0.39	0.65	0.21	0.00	0.03	0.00	**0.16**	0.03	0.05	0.02	0.20	0.02	0.74	0.29	0.01	**2.48**	0.01	0.46	0.10
HIPP	0.02	0.06	0.68	0.13	0.15	0.14	0.17	0.26	0.51	0.00	0.02	0.01	0.22	0.00	0.07	0.13	0.24	0.01	0.61	0.12	0.00	**1.87**	0.00	0.07	0.20
HYPO	0.00	0.00	0.04	0.00	0.03	0.19	0.03	0.02	0.00	0.09	0.00	0.00	0.00	0.01	0.04	0.05	0.00	0.00	0.01	0.04	0.00	0.17	0.12	0.36	0.01
IPL	0.07	0.13	**2.18**	0.00	0.20	**1.13**	**0.78**	0.35	0.18	0.00	0.05	0.02	**0.54**	0.02	0.19	0.10	0.26	0.11	**2.28**	**0.84**	0.00	**4.94**	0.15	**0.96**	0.41
Insula	0.01	0.00	**1.16**	0.05	0.07	0.07	0.41	0.02	0.04	0.00	0.01	0.09	0.19	0.03	0.03	**0.47**	0.03	0.03	0.60	0.22	0.09	1.30	0.00	0.18	0.22
MOG	0.00	0.06	**1.94**	0.07	0.16	0.59	0.54	0.13	0.14	0.00	0.03	0.02	0.81	0.00	0.12	0.26	0.20	0.10	**1.89**	**0.71**	0.04	**3.50**	0.16	**0.69**	0.37
MTG	0.02	0.03	0.02	0.04	0.00	0.32	0.00	0.07	0.00	0.00	0.00	0.01	0.00	0.26	0.00	0.07	0.01	0.00	0.01	0.02	0.02	0.06	0.00	0.03	0.00
Nodule	0.01	0.15	0.52	0.00	0.02	0.38	0.29	0.09	0.08	0.01	0.03	0.01	**0.25**	0.00	0.46	0.07	0.11	0.07	**1.12**	0.31	0.00	1.82	0.05	0.12	0.26
PCC	0.00	0.00	0.70	0.01	0.05	0.14	0.19	0.02	0.07	0.01	0.01	0.04	0.22	0.02	0.03	0.95	0.04	0.02	0.40	0.08	0.07	0.81	0.00	0.07	0.16
PH	0.05	0.10	**1.58**	0.02	**0.24**	**0.88**	0.47	0.37	0.34	0.00	0.04	0.01	**0.48**	0.01	0.12	0.10	0.35	0.05	**1.78**	**0.48**	0.00	**4.12**	0.09	**0.60**	0.43
PTM	0.01	0.05	**1.41**	0.05	0.05	**0.81**	0.59	0.06	0.04	0.00	0.03	0.01	**0.44**	0.00	0.16	0.08	0.10	0.19	**1.66**	**0.65**	0.01	**3.41**	0.26	**0.82**	0.31
RN	0.05	0.07	**1.98**	0.09	0.18	**1.29**	**0.80**	0.17	0.11	0.00	0.04	0.02	**0.54**	0.00	0.16	0.13	0.22	0.10	2.87	**0.86**	0.00	**4.88**	0.27	**1.03**	0.43
SII	0.02	0.06	**2.27**	0.17	0.18	**1.22**	**0.87**	0.17	0.05	0.00	0.04	0.02	**0.53**	0.00	0.11	0.07	0.15	0.11	**2.26**	1.08	0.03	**4.37**	0.29	**1.33**	0.22
SMA	0.09	0.01	0.38	0.15	0.03	0.22	0.08	0.01	0.00	0.00	0.00	0.03	0.14	0.02	0.00	0.25	0.00	0.01	0.04	0.12	0.26	0.09	0.01	0.10	0.02
SN	0.07	0.08	**2.38**	0.03	**0.24**	**1.18**	**0.91**	0.29	0.17	0.00	0.04	0.02	**0.52**	0.00	0.13	0.14	0.27	0.11	**2.56**	**0.87**	0.00	5.66	0.24	**1.22**	0.41
VPLN	0.01	0.01	0.71	0.23	0.06	1.23	0.37	0.01	0.00	0.02	0.01	0.00	0.22	0.00	0.03	0.00	0.05	0.08	**1.33**	**0.54**	0.00	2.19	0.59	**1.22**	0.09
VPMN	0.03	0.02	**1.84**	0.16	0.17	**1.16**	**0.69**	0.16	0.02	0.02	0.03	0.01	**0.31**	0.00	0.03	0.03	0.11	0.08	**1.62**	**0.79**	0.01	**3.64**	0.39	1.84	0.12
Uvula	0.01	0.04	0.94	0.00	0.09	0.24	0.34	0.08	0.12	0.00	0.02	0.02	**0.36**	0.00	0.12	0.18	0.18	0.07	**1.45**	0.28	0.01	**2.64**	0.06	0.25	0.83

Significant paths ($P < 0.05$) are shown in bold.

Hem = hemisphere; ACC = anterior cingulate cortex; AMY = amygdala; CD = caudate; DLPFC = dorsolateral prefrontal cortex; FGM = fastigium; FG = fusiform gyrus; HIPP = hippocampus; HYPO = hypothalamus; IPL = inferior parietal lobule; MOG = middle occipital gyrus; MTG = middle temporal gyrus; PCC = posterior cingulate cortex; PH = parahippocampal gyrus; PTM = putamen; RN = red nucleus; SII = secondary somatosensory cortex; SMA = supplementary motor area; SN = substania nigra; VPLN = ventral posterior lateral nucleus; VPMN = ventral posterior medial nucleus.

Table 3
Path Weights (Arbitrary Units) From Multivariate Granger Causality Analyses of PC7

	ACC	AMY	CD	Culmen	Cuneus	DLPFC	FGM	FG	HIPP	HYPO	IPL	Insula	MOG	MTG	Nodule	PCC	PH	PTM	RN	SII	SMA	SN	VPLN	VPMN	Uvula
ACC	0.12	0.03	0.04	0.00	0.00	0.00	0.01	0.00	0.00	0.00	0.00	0.04	0.00	0.18	0.02	0.00	0.03	0.01	0.10	0.01	0.00	0.01	0.02	0.03	0.04
AMY	0.00	0.85	0.02	0.01	0.00	0.14	0.05	0.00	0.00	0.01	0.07	0.35	0.00	0.07	0.00	0.01	0.03	0.02	0.26	0.00	0.14	0.09	0.26	0.17	0.01
CD	0.01	0.02	0.88	0.00	0.02	0.06	0.24	0.07	0.04	0.01	0.01	0.00	0.25	0.05	0.10	0.17	0.06	0.08	0.01	0.04	0.04	0.12	0.28	0.32	0.00
Culmen	0.00	0.16	0.05	0.08	0.01	0.09	0.36	0.06	0.20	0.00	0.00	0.00	0.00	0.20	0.02	0.11	**1.88**	0.00	**1.49**	0.00	0.18	0.01	0.02	0.00	0.41
Cuneus	0.00	0.00	0.32	0.01	0.02	0.01	0.17	0.05	0.06	0.02	0.02	0.01	0.06	0.00	0.05	0.35	0.39	0.08	0.24	0.01	0.07	0.06	0.32	0.21	0.04
DLPFC	0.00	0.10	0.04	0.01	0.00	1.18	0.03	0.13	0.06	0.01	0.11	0.29	0.00	0.19	0.01	0.00	**1.01**	0.03	0.13	0.00	0.01	0.12	0.15	0.12	0.24
FGM	0.00	0.06	0.36	0.04	0.01	0.05	0.61	0.12	0.23	0.00	0.03	0.00	0.06	0.06	0.08	0.27	**1.51**	0.01	0.48	0.00	0.21	0.06	0.06	0.04	0.24
FG	0.00	0.01	0.14	0.01	0.01	0.33	0.16	0.46	0.05	0.01	0.11	0.18	0.23	0.18	0.03	0.05	0.36	0.03	0.14	0.03	0.00	0.35	0.09	0.13	0.03
HIPP	0.00	0.00	0.09	0.05	0.01	0.22	0.39	0.07	0.35	0.00	0.04	0.02	0.01	0.05	0.07	0.15	**2.94**	0.01	0.80	0.01	0.11	0.05	0.01	0.01	0.42
HYPO	0.00	0.06	0.08	0.00	0.01	0.11	0.00	0.02	0.01	0.16	0.00	0.00	0.03	0.04	0.01	0.00	0.23	0.07	0.07	0.02	0.00	0.04	0.38	0.36	0.00
IPL	0.00	0.24	0.05	0.00	0.00	0.50	0.07	0.20	0.06	0.00	0.25	0.43	0.16	0.04	0.03	0.02	0.44	0.00	0.00	0.01	0.02	**0.37**	0.01	0.00	0.06
Insula	0.01	0.30	0.00	0.00	0.00	0.34	0.00	0.08	0.01	0.00	0.11	1.00	0.07	0.05	0.00	0.05	0.25	0.03	0.00	0.00	0.12	0.19	0.20	0.11	0.01
MOG	0.00	0.01	0.35	0.00	0.01	0.00	0.06	0.17	0.01	0.01	0.07	0.11	0.64	0.01	0.01	0.04	0.01	0.02	0.16	0.02	0.03	0.35	0.07	0.19	0.02
MTG	0.03	0.07	0.05	0.02	0.00	0.27	0.04	0.10	0.02	0.01	0.01	0.05	0.01	0.85	0.00	0.00	0.24	0.00	0.97	0.00	0.02	0.04	0.02	0.01	0.23
Nodule	0.01	0.00	0.47	0.01	0.01	0.07	0.27	0.06	0.13	0.00	0.05	0.00	0.04	0.00	0.19	0.18	0.70	0.03	0.05	0.01	0.11	0.10	0.09	0.09	0.18
PCC	0.00	0.01	0.25	0.01	0.02	0.00	0.27	0.04	0.09	0.00	0.01	0.08	0.04	0.00	0.05	0.62	**0.72**	0.03	0.17	0.00	0.09	0.08	0.14	0.07	0.12
PH	0.00	0.01	0.02	0.04	0.01	0.35	0.27	0.05	**0.30**	0.01	0.03	0.07	0.00	0.06	0.04	0.13	3.38	0.03	0.92	0.01	0.06	0.05	0.08	0.10	0.48
PTM	0.00	0.08	0.28	0.00	0.02	0.13	0.03	0.06	0.01	0.05	0.00	0.13	0.06	0.01	0.02	0.08	0.46	0.23	0.00	0.05	0.04	0.02	**0.79**	**0.67**	0.03
RN	0.01	0.09	0.00	0.04	0.01	0.07	0.13	0.03	0.12	0.00	0.00	0.00	0.04	0.36	0.00	0.05	**1.35**	0.00	2.26	0.01	0.10	0.00	0.03	0.00	0.36
SII	0.01	0.00	0.27	0.00	0.01	0.01	0.02	0.11	0.02	0.02	0.01	0.00	0.11	0.00	0.02	0.00	0.37	0.11	0.16	0.11	0.00	0.03	0.29	0.33	0.08
SMA	0.00	0.25	0.08	0.03	0.01	0.03	0.27	0.00	0.08	0.00	0.01	0.27	0.03	0.03	0.04	0.12	0.41	0.02	0.51	0.00	0.45	0.09	0.12	0.04	0.19
SN	0.00	0.10	0.15	0.00	0.00	0.18	0.05	0.22	0.03	0.01	0.12	0.26	0.30	0.04	0.02	0.07	0.23	0.01	0.00	0.00	0.06	0.68	0.03	0.06	0.04
VPLN	0.00	0.22	0.25	0.00	0.03	0.20	0.04	0.04	0.00	0.06	0.00	0.21	0.04	0.02	0.02	0.09	0.28	0.20	0.06	0.03	0.06	0.02	0.97	**0.79**	0.01
VPMN	0.00	0.17	0.32	0.00	0.02	0.16	0.03	0.07	0.00	0.07	0.00	0.14	0.14	0.01	0.02	0.05	0.41	0.19	0.00	0.04	0.02	0.05	**0.87**	0.86	0.03
Uvula	0.01	0.01	0.00	0.04	0.00	0.36	0.19	0.02	0.19	0.00	0.02	0.01	0.01	0.25	0.04	0.09	**2.08**	0.01	**1.05**	0.01	0.11	0.04	0.01	0.03	0.78

Significant paths ($P < 0.05$) are shown in bold.

Hem = hemisphere; ACC = anterior cingulate cortex; AMY = amygdala; CD = caudate; DLPFC = dorsolateral prefrontal cortex; FGM = fastigium; FG = fusiform gyrus; HIPP = hippocampus; HYPO = hypothalamus; IPL = inferior parietal lobule; MOG = middle occipital gyrus; MTG = middle temporal gyrus; PCC = posterior cingulate cortex; PH = parahippocampal gyrus; PTM = putamen; RN = red nucleus; SII = secondary somatosensory cortex; SMA = supplementary motor area; SN = substania nigra; VPLN = ventral posterior lateral nucleus; VPMN = ventral posterior medial nucleus.

Table 4
Path Weights (Arbitrary Units) From Multivariate Granger Causality Analyses of GB37

	ACC	AMY	CD	Culmen	Cuneus	DLPFC	FGM	FG	HIPP	HYPO	IPL	Insula	MOG	MTG	Nodule	PCC	PH	PTM	RN	SII	SMA	SN	VPLN	VPMN	Uvula
ACC	0.05	0.15	0.00	0.04	0.05	0.12	0.02	0.06	0.10	0.00	0.00	0.02	0.02	0.02	0.18	0.14	0.01	0.00	0.13	0.00	0.01	0.09	0.00	0.02	0.05
AMY	0.01	0.73	0.00	0.08	0.15	0.10	0.00	0.07	0.03	0.05	0.05	0.01	0.04	0.05	0.02	0.01	0.37	0.01	0.03	0.11	0.09	0.06	0.04	0.00	0.06
CD	0.00	0.00	0.65	0.04	0.26	0.23	0.01	0.29	0.04	0.00	0.29	0.00	0.01	0.13	0.15	0.01	0.00	0.04	0.34	0.02	0.52	0.15	0.38	0.00	0.01
Culmen	0.01	0.26	0.13	0.21	0.01	0.04	0.01	0.05	0.01	0.01	0.12	0.00	0.01	0.00	0.00	0.00	0.03	0.03	0.10	0.01	0.07	0.00	0.06	0.00	0.00
Cuneus	0.00	0.08	0.12	0.00	1.34	0.07	0.02	0.32	0.00	0.01	0.16	0.02	0.05	0.21	0.24	0.22	0.12	0.00	0.00	0.06	0.46	0.33	0.28	0.00	0.07
DLPFC	0.01	0.08	0.18	0.01	0.10	0.83	0.00	0.50	0.06	0.04	0.02	0.00	0.00	0.06	0.00	0.05	0.33	0.00	0.30	0.11	0.50	0.49	0.33	0.01	0.05
FGM	0.01	0.03	0.04	0.01	0.27	0.01	0.12	0.03	0.06	0.00	0.03	0.01	0.04	0.04	0.12	0.06	0.00	0.00	0.03	0.00	0.02	0.07	0.16	0.04	0.04
FG	0.00	0.06	0.21	0.01	0.48	**0.48**	0.00	0.88	0.01	0.02	0.11	0.00	0.03	0.18	0.05	0.00	0.28	0.00	0.12	0.15	**0.86**	0.62	0.54	0.00	0.18
HIPP	0.01	0.04	0.06	0.00	0.00	0.12	0.01	0.01	0.46	0.05	0.08	0.00	0.01	0.00	0.12	0.06	0.29	0.02	0.01	0.03	0.01	0.19	0.04	0.02	0.08
HYPO	0.00	0.21	0.00	0.01	0.09	0.20	0.00	0.11	0.11	0.19	0.03	0.00	0.00	0.05	0.00	0.00	0.36	0.00	0.02	0.13	0.14	0.30	0.13	0.00	0.08
IPL	0.00	0.07	0.36	0.05	0.41	0.04	0.01	0.20	0.06	0.01	0.52	0.01	0.00	0.13	0.21	0.10	0.03	0.04	0.15	0.00	0.39	0.08	0.19	0.00	0.02
Insula	0.02	0.09	0.04	0.00	0.79	0.00	0.01	0.07	0.04	0.02	0.11	0.03	0.04	0.17	0.37	0.30	0.01	0.00	0.09	0.03	0.18	0.06	0.14	0.01	0.00
MOG	0.00	0.14	0.03	0.01	0.32	0.01	0.02	0.15	0.02	0.00	0.00	0.01	0.20	0.11	0.10	0.07	0.11	0.00	0.03	0.05	0.16	0.10	0.23	0.01	0.09
MTG	0.00	0.10	0.23	0.00	0.81	0.14	0.01	0.44	0.00	0.02	0.19	0.02	0.06	0.36	0.29	0.13	0.19	0.00	0.00	0.13	**0.80**	0.42	0.36	0.00	0.03
Nodule	0.02	0.02	0.17	0.00	0.57	0.00	0.02	0.07	0.09	0.00	0.19	0.03	0.04	0.18	0.59	0.18	0.00	0.01	0.00	0.02	0.31	0.03	0.16	0.01	0.00
PCC	0.01	0.01	0.02	0.00	0.65	0.10	0.01	0.01	0.06	0.00	0.12	0.03	0.03	0.10	0.23	0.44	0.01	0.00	0.18	0.00	0.06	0.00	0.03	0.01	0.00
PH	0.00	0.33	0.00	0.01	0.19	0.34	0.00	0.30	0.15	0.08	0.02	0.00	0.03	0.08	0.00	0.01	0.84	0.02	0.00	0.16	0.31	0.45	0.14	0.00	0.21
PTM	0.00	0.13	0.26	0.06	0.03	0.00	0.00	0.00	0.09	0.01	0.27	0.00	0.01	0.01	0.08	0.02	0.24	0.07	0.22	0.01	0.05	0.01	0.06	0.00	0.14
RN	0.01	0.02	0.22	0.02	0.00	0.26	0.00	0.10	0.01	0.00	0.08	0.00	0.01	0.00	0.00	0.08	0.00	0.02	0.99	0.00	0.13	0.10	0.09	0.01	0.00
SII	0.00	0.33	0.04	0.01	0.34	0.39	0.00	**0.52**	0.05	0.10	0.00	0.01	0.04	0.18	0.04	0.00	0.52	0.00	0.00	0.25	**0.70**	0.53	0.32	0.00	0.15
SMA	0.00	0.06	0.30	0.01	0.56	0.38	0.00	**0.68**	0.00	0.02	0.18	0.01	0.03	0.25	0.16	0.02	0.24	0.00	0.11	0.16	1.11	0.47	0.46	0.00	0.05
SN	0.01	0.05	0.11	0.00	0.47	**0.44**	0.01	**0.58**	0.09	0.06	0.04	0.00	0.02	0.17	0.02	0.00	0.41	0.00	0.10	0.15	0.56	0.96	0.43	0.00	0.19
VPLN	0.00	0.03	0.29	0.01	0.44	0.33	0.02	**0.54**	0.02	0.03	0.12	0.01	0.05	0.15	0.11	0.01	0.13	0.01	0.10	0.09	**0.59**	0.45	0.85	0.01	0.07
VPMN	0.01	0.02	0.00	0.00	0.03	0.07	0.05	0.02	0.12	0.00	0.01	0.00	0.02	0.00	0.05	0.05	0.01	0.00	0.08	0.00	0.05	0.02	0.07	0.08	0.01
Uvula	0.00	0.08	0.01	0.00	0.19	0.09	0.01	0.31	0.07	0.03	0.02	0.00	0.03	0.02	0.00	0.00	0.35	0.02	0.00	0.07	0.10	0.34	0.13	0.00	0.50

Significant paths ($P < 0.05$) are shown in bold.

Hem = hemisphere; ACC = anterior cingulate cortex; AMY = amygdala; CD = caudate; DLPFC = dorsolateral prefrontal cortex; FGM = fastigium; FG = fusiform gyrus; HIPP = hippocampus; HYPO = hypothalamus; IPL = inferior parietal lobule; MOG = middle occipital gyrus; MTG = middle temporal gyrus; PCC = posterior cingulate cortex; PH = parahippocampal gyrus; PTM = putamen; RN = red nucleus; SII = secondary somatosensory cortex; SMA = supplementary motor area; SN = substania nigra; VPLN = ventral posterior lateral nucleus; VPMN = ventral posterior medial nucleus.

between a seed region and any other brain structures throughout the whole brain, depicting brain networks related to certain functions. However, this method was limited to assess brain regions functionally connected to the initially selected seed and was unable to directly characterize interactions between multiple brain regions. In this study, we addressed this problem by introducing the mGCA to detect causal influences between multiple brain areas. By visualizing the effective connectivity, we can obtain both the direction and strength of the information flow between multiple brain regions in the resting state network.

From the mGCA results, we identified that brain regions have extensive causal interactions following acupuncture at PC6, mainly locating at the amygdala, caudate, fastigium, hippocampus, insula, PH, and flocculonodular lobe of cerebellum (nodule and uvula). Previous studies from Hui and colleagues also demonstrated that these brain regions can be modulated by acupuncture (3,20). These limbic-cerebellum and subcortical areas are more engaged in affective motivation and autonomic drive of bodily responses (29). Therefore, the causal influences between these brain regions may be related to the sedative or tranquilizing effect of PC6 after a variety of stressors or depression (17). It was also worth noting that several limbic/paralimbic-cerebellum areas (the fastigium, hippocampus, PH, uvula) also have causal interactions underlying acupuncture at PC7 in the poststimulus rest brain networks. Even with the relative similarity, the PH was presented to be the most important brain areas, receiving causal inflows mainly from the hippocampus. These stress-sensitive brain regions have previously been reported for their central role in depressive illness (30). The causal influences between the PH and other brain regions underlying PC7 may provide an explanation for the mediate effect of PC7 to treat depressive disorders (31).

In addition, we identified the insula and nodule have causal interactions with other brain regions only following acupuncture at PC6. Previous studies in humans have reported that resection of the insula resulted in visceral motor dysfunction, nausea, vomiting and gastrointestinal disorders (32). Therefore, the causal influences anchored by insula may help better understand the specific treatment effect of PC6 on the nausea and vomiting. The flocculonodular lobe of the nodule, as part of vestibule cerebellum, receives vestibular projections from primary and secondary vesibular afferents, as well as vestibular climbing fibers (33,34). Our study demonstrated that the causal patterns underlying acupoint PC6 in the treatment of nausea can selectively modulate specific neural substrates—the flocculonodular lobe of nodule related to vestibular function, subsequently alleviating the symptoms with motion-related sickness and nausea (4).

Along the different meridian with respect to PC6, the GB37 was an acupoint belonging to the gallbladder channel. As its name "brightness" suggests, GB37 was described as a very effective acupoint influencing multiple vision-related disorders, such as the cataracts, night blindness and optic atrophy (19). The mGCA result demonstrated that acupuncture at this acupoint saliently elicited different effective connectivity compared with PC6 and PC7. The brain regions with extensive causal interactions were primarily located at the vision-related cortex (the fusiform gyrus), with limited extent of the limbic system. The fusiform gyrus became an important site of target, receiving major inputs from both the SII and thalamus (VPLN, VPMN). The drive from the SII to the fusiform gyrus intuitively depicted that there existed a control signal starting from the somatosensory cortex to the vision-related cortex, thereby elucidating the treatment of GB37 in vision-related disorders. Results indicated that acupuncture at acupoints along different meridian may induce distinct reorganization of the effective connectivity across different neural subsystems.

In conclusion, our findings demonstrated that there existed different effective connectivity patterns during the poststimulus resting state following acupuncture at acupoint PC6, compared with the same meridian acupoint PC7 and different meridian acupoint GB37. We suggested that the distinct modulation patterns of the resting brain attributed to the specific effects evoked by the three acupoints. We also identified that some important brain regions emerged as central hubs in the poststimulus resting brain. These brain regions may be related to the effects of acupoint on modulating special disorder treatment. This preliminary finding may provide a new clue to understand the relatively function-oriented specificity of acupuncture effects.

REFERENCES

1. NIH. NIH consensus conference statement acupuncture. JAMA 1998;280:1518–1524.
2. Fang JL, Jin Z, Wang Y, et al. The salient characteristics of the central effects of acupuncture needling: limbic-paralimbic-neocortical network modulation. Hum Brain Mapp 2009;30: 1196–1206.
3. Hui KK, Liu J, Makris N, et al. Acupuncture modulates the limbic system and subcortical gray structures of the human brain: evidence from fMRI studies in normal subjects. Hum Brain Mapp 2000;9:13–25.
4. Yoo SS, Teh EK, Blinder RA, Jolesz FA. Modulation of cerebellar activities by acupuncture stimulation: evidence from fMRI study. Neuroimage 2004;22:932–940.
5. Beijing S. Nanjing colleges of traditional Chinese medicine. Essentials of Chinese acupuncture. Beijing: Foreign Language Press; 1980:36.
6. Bai LJ, Qin W, Tian J, et al. Time-varied characteristics of acupuncture effects in fMRI studies. Hum Brain Mapp 2009;30: 3445–3460.
7. Bai LJ, Yan H, Li L, et al. Neural specificity of acupuncture stimulation at pericardium 6: evidence from an FMRI study. J Magn Reson Imaging 2010;31:71–77.
8. Bai LJ, Qin W, Tian J, et al. Acupuncture modulates spontaneous activities in the anticorrelated resting brain networks. Brain Res 2009;1279:37–49.
9. Bai LJ, Tian J, Zhong C, et al. Acupuncture modulates temporal neural responses in wide brain networks: evidence from fMRI study. Mol Pain 2010;6:73.
10. Bai LJ, Qin W, Liang JM, Tian J, Liu YJ. Spatiotemporal modulation of central neural pathway underlying acupuncture action: a systematic review. Curr Med Imaging Rev 2009;5:167–173.
11. Dhond RP, Yeh C, Park K, Kettner N, Napadow V. Acupuncture modulates resting state connectivity in default and sensorimotor brain networks. Pain 2008;136:407–418.

12. Bai LJ, Qin W, Tian J, Dai JP, Yang WH. Detection of dynamic brain networks modulated by acupuncture using a graph theory model. Prog Nat Sci 2009;19:827–835.
13. Deshpande G, LaConte S, James GA, Peltier S, Hu X. Multivariate Granger causality analysis of fMRI data. Hum Brain Mapp 2009;30:1361–1373.
14. Deshpande G, LaConte S, Peltier S, Hu X. Directed transfer function analysis of fMRI data to investigate network dynamics. Conf Proc IEEE Eng Med Biol Soc 2006;1:671–674.
15. Stilla R, Deshpande G, LaConte S, Hu X, Sathian K. Posteromedial parietal cortical activity and inputs predict tactile spatial acuity. J Neurosci 2007;27:11091–11102.
16. Oldfield RC. The assessment and analysis of handedness: the Edinburgh inventory. Neuropsychologia 1971;9:97–113.
17. Stux. G, Pomeranz. B. Acupuncture: textbook and atlas. Berlin: Springer-Verlag; 1987. p 231–244.
18. Dundee JW, Chestnutt WN, Ghaly RG, Lynas AG. Traditional Chinese acupuncture: a potentially useful antiemetic. BMJ 1986; 293:583–584.
19. Liu GW. Acupoints of three Yang meridians of foot. In: Liu GW, editor. A complement work of present acupuncture and moxibustion. Tianjin: Hua Xia Publishing House; 1997:327–479.
20. Hui KK, Liu J, Marina O, et al. The integrated response of the human cerebro-cerebellar and limbic systems to acupuncture stimulation at ST 36 as evidenced by fMRI. Neuroimage 2005;27: 479–496.
21. Kong J, Gollub R, Huang T, et al. Acupuncture de qi, from qualitative history to quantitative measurement. J Altern Complement Med 2007;13:1059–1070.
22. Ashburner J, Friston KJ. Nonlinear spatial normalization using basis functions. Hum Brain Mapp 1999;7:254–266.
23. Blinowska KJ, Kus R, Kaminski M. Granger causality and information flow in multivariate processes. Phys Rev E Stat Nonlin Soft Matter Phys 2004;70:50902–50906.
24. Akaike H. New look at statistical-model identification. IEEE Trans Automat Contr 1974;19:716–723.
25. Kus R, Kaminski M, Blinowska KJ. Determination of EEG activity propagation: pair-wise versus multichannel estimate. IEEE Trans Biomed Eng 2004;51:1501–1510.
26. Strang G. Introduction to linear algebra. Cambridge: Wellesley-Cambridge Press; 1998.
27. Theiler J, Eubank S, Longtin A, Galdrikian B, Farmer JD. Testing for nonlinearity in time-series - the method of surrogate data. Physica D 1992;58:77–94.
28. Jiao Q, Lu G, Zhang Z, et al. Granger causal influence predicts BOLD activity levels in the default mode network. Hum Brain Mapp 2011;32:154–161.
29. Mann F. Reinventing acupuncture: a new concept of ancient medicine. Great Britain: Biddles Ltd; 1992. 44 p.
30. Campbell S, Macqueen G. The role of the hippocampus in the pathophysiology of major depression. J Psychiatry Neurosci 2004;29:417–426.
31. McDonald B, Highley JR, Walker MA, et al. Anomalous asymmetry of fusiform and parahippocampal gyrus gray matter in schizophrenia: a postmortem study. Am J Psychiatry 2000;157:40–47.
32. Penfield W, Jasper HH. Epilepsy and the functional anatomy of the human brain. New York: Little, Brown and Company; 1954.
33. Ito M. Neurophysiology of the nodulofloccular system. Rev Neurol (Paris) 1993;149:692–697.
34. Pettorossi VE, Grassi S, Errico P, Barmack NH. Role of cerebellar nodulus and uvula on the vestibular quick phase spatial constancy. Acta Otolaryngol Suppl 2001;545:155–159.